2022

Balancing Supercapacitor Voltages in Modular Bidirectional DC–DC Converter Circuits

Robert Alfie S. Peña
Ateneo de Manila University, rpena@ateneo.edu

Alaa Hijazi
Université Claude Bernard Lyon

Pascal Venet
Université Claude Bernard Lyon

Florian Errigo
Université Claude Bernard Lyon

Recommended Citation

Pena, R. A. S., Hijazi, A., Venet, P., & Errigo, F. (2022). Balancing Supercapacitor Voltages in Modular Bidirectional DC–DC Converter Circuits. IEEE Transactions on Power Electronics, 37(1), 137–149. https://doi.org/10.1109/TPEL.2021.3093767

Balancing Supercapacitor Voltages in Modular Bidirectional DC-DC Converter Circuits

Robert Alfie S. Peña, Alaa Hijazi, Pascal Venet, *Member, IEEE,* and Florian Errigo

***Abstract*—At present, passive balancing methods dominate energy storage applications, however they suffer from a long balancing duration. In this paper, we took advantage of a modular architecture where several modular power converters replace a central dc-dc converter for fast charging and balancing of a supercapacitor stack. A strategy has been proposed to control how power is shared among the converters during the charging period in order to balance the supercapacitors. However, some converters enter control saturation due to voltage differences between supercapacitors caused by their nonuniform conditions and characteristics. The originality of this paper lies in taking into account the saturation by modifying an energy-based strategy to correct the power shares and make balancing the supercapacitors possible. Simulation and experimental case studies were used to demonstrate the strategy's performance and limitations.**

***Index Terms*—Balancing circuit, balancing strategy, charging supercapacitors, DC-DC power converter, power control, supercapacitors.**

I. Introduction

ENERGY storage plays a huge role in a future where energy is more integrated, decentralized, and sustainable. In general, we use energy storage devices with high energy density like batteries for bulk energy storage and devices with high power density like supercapacitors as buffer in high power transient situations [1], [2].

Supercapacitors, also called ultracapacitors or electrical double-layer capacitors (EDLC), have a much higher charge storage capability compared to the usual types of capacitors because of the large surface area of the porous electrodes and the extremely thin electrical double layer [1], [3]–[6]. Compared to batteries, supercapacitors have a longer lifetime because no electrochemical reaction causes significant degradation permitting excellent reversibility and higher charge-discharge cycles [1], [3], [4], [6].

Even though supercapacitors have high power densities, their low operating voltages are limited for use in most applications. Thus, cells are connected in series, in parallel, and/or in combination to reach requirements [1]. Since supercapacitor characteristics are never fully uniform even with today's advanced manufacturing processes, the choice of connection limits the electrical behavior of the cells. This initial imbalance then exacerbates during operation because of the uneven aging of the cells [7]–[9]. Thus, there is a need for a system that balances the cell voltages to ensure the safe operation and a prolonged lifetime for supercapacitors [1], [3], [7]. This requires energy storage management systems that also monitor voltages, currents, and temperatures, and that interface with other devices [1], [2].

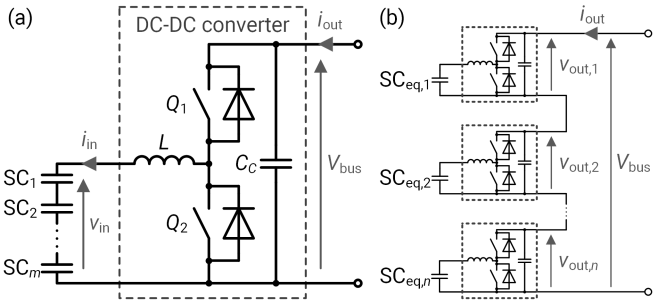

Fig. 1. Supercapacitor power conversion systems: (a) A single nonisolated bidirectional dc-dc converter interfacing a supercapacitor stack at the low side ($V_{\rm bus} \geq v_{\rm in}$) and (b) Modular power converters interfacing supercapacitor groupings

In the literature, there are two types of balancing circuits: passive or dissipative and active or redistributive. In passive balancing, the excess charge in the cells is dissipated through resistors. It is the simplest and cheapest strategy to implement. On the other hand, active balancing redistributes charge from overcharged to undercharged cells, which is more efficient. Although costs depend a lot on the chosen architecture, this strategy is commonly expensive to implement because of additional components and the more complicated control systems [9]–[12]. Recently, a third approach in balancing emerged. It capitalizes on the energy management systems of modular dc-dc power converters that interface the energy storage devices with the rest of the system. Like active balancing, it is nondissipative, but unlike both the first two types, there is no need for separate balancing circuits connected in parallel because balancing can be integrated in the same algorithms that control the output voltages of the connected converters. DC bus voltage regulation and balancing without the extra circuitry or charge redistribution are thus possible in an efficient, modular way [13]–[20].

The nonisolated bidirectional dc-dc converter in Fig. 1(a), whose output voltage $V_{\rm bus} \geq v_{\rm in}$ (its input voltage), is com-

The work of R. A. S. Peña was supported by the Philippine Commission on Higher Education (CHED) and the Embassy of France to the Philippines through a CHED-PhilFrance Scholarship. The experimental part of this work was supported by the French National Research Agency (ANR) under the Programme d'investissements d'avenir (ANE-ITE-002-01).

The authors are with the Université de Lyon, Université Claude Bernard Lyon 1, INSA Lyon, Ecole Centrale de Lyon, CNRS, Ampère, UMR5005, 69622 Villeurbanne, France and also with the SuperGrid Institute, 69628 Villeurbanne, France (e-mail: robert.pena@etu.univ-lyon1.fr; alaa.hijazi@insa-lyon.fr; pascal.venet@univ-lyon1.fr; florian.errigo@supergrid-institute.com).

R. A. S. Peña is also with the Department of Electronics, Computer, and Communications Engineering, Ateneo de Manila University, 1108 Quezon City, Philippines (e-mail: rpena@ateneo.edu).

monly used to interface supercapacitors with different applications [21]–[25]. It is in boost mode when the supercapacitors are discharging and in buck mode when the supercapacitors are charging. In case of a relatively high-voltage bus, low-voltage supercapacitor cells are placed in series at the low side of the converter, while the high side is directly connected to the dc bus [24]. Cascading these converters as in Fig. 1(b) has recently been employed to meet dc bus voltage requirements.

The half-bridge modular architecture of Fig. 1(b) was chosen in consideration of two related previous studies [26]–[28]. The first study aimed at recovering the braking energy of trolleybuses and storing them in supercapacitors. A central converter as in Fig. 1(a) was used to interface the supercapacitors that served as auxiliary supply to the rest of the powertrain during power cuts in the operation of a trolleybus [26]. The new modular architecture in Fig. 1(b) allows a new degree of flexibility in terms of control that is beneficial for managing electrothermal imbalances. The concern in the modular architecture was to have the (relatively) simplest structure and control system to minimize the number of components and to have lower bias range for these components. The approach of modularizing the topology balloons the number of basic components, so the choice of topology was just generally optimizing for anticipated costs. On the other hand, the second study is about the integration of supercapacitors into modular multilevel converters (MMC), which is composed of hundreds of submodules [27]. The architecture in Fig. 1(b) was proposed as an interface between supercapacitors and the submodule capacitors of the MMC [28]. In this second study, the advantage of the interfacing modular architecture is to provide submodules with an energy storage function with a higher power density and compact passive components.

The architecture offers modularity that provides increased overall reliability and flexibility to the system [29]. Nonetheless, when charging unbalanced supercapacitors to reach the same voltage (balancing) using the circuit of Fig. 1(b), the unique problem of saturation in the control of a modular converter j through the duty ratio D_j arises on account of the possible overlap of the voltage ranges of unbalanced supercapacitors and the high side of the converter. This occurs because a low conversion ratio $M_j\,(D_j) = v_{\mathrm{sc},j}/v_{\mathrm{out},j}$ for the modular converters in buck mode in Fig. 1(b) is impractical, which would otherwise have provided the voltage margin necessary to skirt the problem [30]. This will be shown in subsection A in section IV to be due to the D_j range limiting the acceptable converter efficiency. Another factor in the problem is that unlike batteries, which have comparatively flat voltage curves relative to their state of charge, supercapacitor voltage varies from 0 to $V_{\max}$ (supercapacitor maximum rated voltage) relative to its state of energy, with operation usually limited to $V_{\max}/2$ to $V_{\max}$. This adds to the probability of overlap. Control saturation will be explained in detail in the next section.

A survey of the literature shows a great number of different state-of-charge- or voltage-balancing strategies, mostly for batteries [9]–[12], [14], [15], [18], [24]. While they can also be used for supercapacitors, unfortunately, they are slow and could take anywhere from a couple to hundreds of minutes

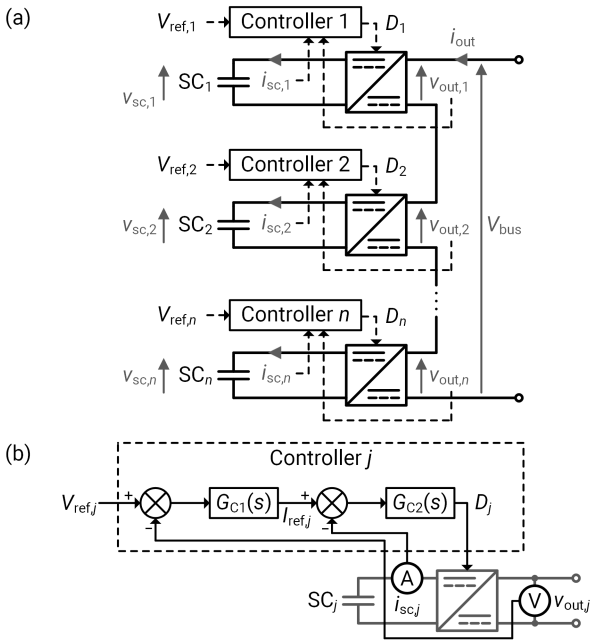

Fig. 2. The control system to charge/discharge supercapacitors using modular power converters: (a) System-level control and (b) Module-level control

to achieve equalization. Considering fast balancing, no study has yet tackled the previously described problem of control saturation that result from the converter architecture and the supercapacitor characteristics. We address this inadequacy in the literature through a method of balancing supercapacitor voltages in modular power electronic converter circuits within, if possible, a single charging period. We propose to use the strategy here in applications where supercapacitors are needed as power buffer like in electric vehicles or in grid-integrated energy storage systems [21]–[26]. Only occasional voltage balancing would then be needed. This is possible because voltage imbalances would be minimal if cell characteristics were ensured to be reasonably uniform from the start [31].

The paper is organized in six sections. The voltage-balancing strategy and the problem of saturation in the control of modular power converters will be explicated in the next section (II). Section III presents the control saturation-adapted strategy. Then, the system setup and the case studies that demonstrate the operation of the strategy will be discussed in sections IV and V. The last section (VI) concludes the paper.

II. Saturation of Modular Converter Control

In this section, we introduce the problem of saturation in the control of modular power converters, however we will first describe in detail the circuits, control systems, and models involved.

A. Control Systems

Fig. 2(a) shows the control architecture at the system level. Modular power converters are cascaded such that the total converter output voltage $\sum_{j=1}^{n} v_{\mathrm{out},j} = V_{\mathrm{bus}}$ is regulated, where $j \in (1, 2, \ldots, n)$ is the index and n is the total number

of converters. Each converter has its own controller that has $V_{\mathrm{ref},j}$ as reference voltage and $v_{\mathrm{out},j}$ as the output controlled by a pulse width modulated (PWM) control signal with duty ratio $D_j \in [0,1]$.

The architecture of the controllers is shown in detail in Fig. 2(b). It is a conventional two-loop control system that responds to disturbances and corrects nonlinearities better than a single-loop system. The slower outer loop (with a response time $t_{\mathrm{r}} = 5$ ms that is the time required by the response to settle within 5% of the final value) is for controlling the converter output voltage, which is the capacitor voltage, while the faster inner one (with a response time $t_{\mathrm{r}} = 1$ ms) is for controlling the converter input current, which is the inductor current (also the converter input current) in Fig. 1(a). In order to use this two-loop control system, the open-loop control-to-output transfer function $G_{v_{\mathrm{out}}d}(s)$ representing the converter must be decomposed into two transfer functions: the control-to-input current transfer function $G_{i_{\mathrm{in}}d}(s)$ and the input current-to-output voltage transfer function $G_{v_{\mathrm{out}}i_{\mathrm{in}}}(s)$ through state space average modelling [32]. Desired are the resulting transfer functions (with the hat denoting an ac small signal):

$$G_{i_{\mathrm{in}}d}(s) = \frac{\widehat{i_{\mathrm{in}}}(s)}{\hat{d}(s)} = \frac{C_C V_{\mathrm{out}} s - I_{\mathrm{out}}}{LC_C s^2 + D^2} \tag{1}$$

$$G_{v_{\mathrm{out}}i_{\mathrm{in}}}(s) = \frac{\widehat{v_{\mathrm{out}}}(s)}{\widehat{i_{\mathrm{in}}}(s)} = \frac{I_{\mathrm{in}} L s + D V_{\mathrm{out}}}{-V_{\mathrm{out}} C_C s + D I_{\mathrm{in}}} \tag{2}$$

whose parameter values are discussed in subsection A in section IV.

The transfer functions in (1) and (2) were used to obtain the proportional-plus-integral (PI) controllers $G_{\mathrm{C1}}(s)$ and $G_{\mathrm{C2}}(s)$. In the outer loop, the error between $V_{\mathrm{ref},j}$ and the measured feedback $v_{\mathrm{out},j}$ (output of (2) in the model) feeds into controller $G_{\mathrm{C1}}(s)$, which outputs the reference value for the inductor current $I_{\mathrm{ref},j}$. In the inner loop, the error between this $I_{\mathrm{ref},j}$ and the measured supercapacitor current feedback $i_{\mathrm{sc},j}$ (output of (1) in the model) feeds into controller $G_{\mathrm{C2}}(s)$, which then outputs the duty ratio of the PWM control signal to the converter.

If the supercapacitor voltages $v_{\mathrm{sc},j}$ are balanced, $V_{\mathrm{ref},j} = V_{\mathrm{ref,total}}/n$, where $V_{\mathrm{ref,total}}$ is the sum of all reference voltages and can be considered the reference bus voltage. Otherwise, a difference between the reference voltages can be used to control the system in order to balance the supercapacitor voltages. A strategy exactly doing this will be presented in the next section.

B. Supercapacitors

Supercapacitors can be modeled in several ways. The simplest is the RC model shown in Fig. 3(a), which is composed of a constant capacitance C_{sc} that serves as the energy storage element in series with a resistance R_{sc} that represents the equivalent series resistance (ESR) of supercapacitors. More complex accurate models build on this one. In this work, however, we are mainly concerned with the steady state behavior of supercapacitors. Thus, a macroscopic model such as the RC model suffices [33]–[35].

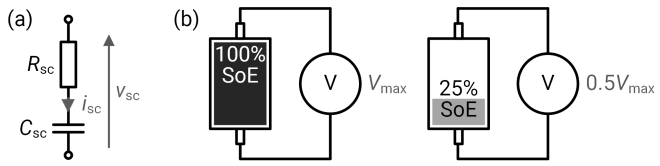

Fig. 3. Supercapacitor model and state: (a) The RC model of a cell and (b) The relationship between the state of energy (SoE) and voltage

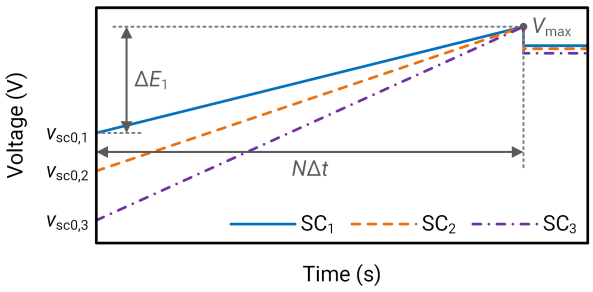

Fig. 4. Balancing the voltages of three supercapacitors to reach V_{max}; SC_1 must be charged with the energy ΔE_1

As mentioned, energy is stored in the capacitor component of the supercapacitor RC model. As such, it is given by:

$$E = \frac{1}{2} C_{\mathrm{sc}} v_{\mathrm{sc}}^2 \tag{3}$$

where E is the energy (J) and v_{sc} is the supercapacitor voltage. Strictly speaking, the latter is the open-circuit voltage, but throughout this paper, we approximate it to be just the supercapacitor voltage because $|v_{R\mathrm{sc}}| \ll |v_{C\mathrm{sc}}|$, where $v_{R\mathrm{sc}}$ is the voltage across R_{sc} and $v_{C\mathrm{sc}}$ is the voltage across C_{sc} in Fig. 3(a). The state of energy (SoE) then, relative to a supercapacitor maximum rated voltage V_{max}, is [5], [36], [37]:

$$SoE = \left(\frac{v_{\mathrm{sc}}}{V_{\mathrm{max}}} \right)^2 \times 100 \tag{4}$$

Eq. (4) shows that the SoE range from 0% to 100% is a square function of the supercapacitor voltage range from 0 V up to V_{max}. The operational SoE range, shown in Fig. 3(b), is usually limited from 25% to 100% to have a usable voltage range between half the rated voltage ($V_{\mathrm{max}}/2$) up to V_{max}. This allows use of 75% of stored energy [5].

C. Voltage-Balancing Strategy

The important goals for the balancing strategy is (i) to charge the supercapacitors until they reach the maximum rated voltage V_{max}, and (ii) to reach this full charge at the same time. These are illustrated in Fig. 4, where there are three supercapacitor voltages that need to be balanced. For a supercapacitor j to reach V_{max} at the end, it must be charged with the amount of energy:

$$\Delta E_j(t) = \frac{1}{2} C_{\mathrm{sc},j} \left[V_{\mathrm{max}}^2 - v_{\mathrm{sc},j}^2(t) \right] \tag{5}$$

The average power of supercapacitor SC_j during the charging period $N\Delta t$, where N is the number of time steps, is:

$$P_j = \frac{\Delta E_j}{N \Delta t} \tag{6}$$

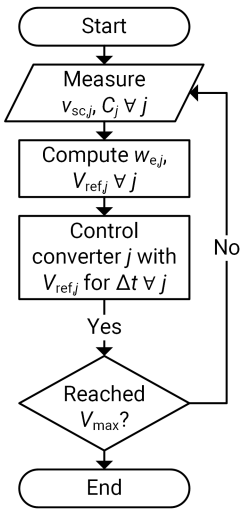

Fig. 5. Flowchart of the voltage-balancing strategy algorithm

Bearing in mind the second objective for the balancing strategies, $N\Delta t$ should be the same for all supercapacitors. We can thus solve for $N\Delta t$ in (6) and the resulting ratio of energy and power should be the same for all n supercapacitors:

$$\frac{\Delta E_j}{P_j} = \frac{\Delta E_{j+1}}{P_{j+1}} = \cdots = \frac{\Delta E_n}{P_n} \tag{7}$$

In Fig. 2(a), we can see that the converters have the same output current i_{out}. We assume ideal converters, which means that the ratio of energy and output voltage should also be the same for all supercapacitors:

$$\frac{\Delta E_j}{v_{\text{out},j}} = \frac{\Delta E_{j+1}}{v_{\text{out},j+1}} = \cdots = \frac{\Delta E_n}{v_{\text{out},n}} \tag{8}$$

We would like the strategy to have the form where the power of converter j is shown as a share of the voltage regulation at the output. To do this, we define and generalize a weighting factor w_j as the ratio of $\Delta E_j\,(t)$ and the total charging energy:

$$w_j\,(t) = \frac{\Delta E_j\,(t)}{\sum_{m=1}^{n} \Delta E_m\,(t)} \tag{9}$$

Multiplying (8) by the reciprocal of the total charging energy, we obtain:

$$\frac{w_j}{v_{\text{out},j}} = \frac{w_{j+1}}{v_{\text{out},j+1}} = \cdots = \frac{w_n}{v_{\text{out},n}} \tag{10}$$

To express $v_{\text{out},j}$ in terms of the weighting factor and the total output voltage V_{bus}, we note that:

$$V_{\text{bus}} = \frac{\sum_{j=1}^{n} v_{\text{out},j}}{\sum_{j=1}^{n} w_j} \tag{11}$$

where the denominator is just equal to unity. We can solve for $v_{\text{out},j+1}$, $v_{\text{out},j+2}$, …, $v_{\text{out},n}$ in terms of $v_{\text{out},j}$ in (10) and substitute them into (11). Doing that, rearranging, and considering that $V_{\text{ref,total}}$ is the reference bus voltage and $V_{\text{ref},j} = v_{\text{out},j}$ at steady state:

$$V_{\text{ref},j}\,(t) = V_{\text{ref,total}} w_j\,(t) \tag{12}$$

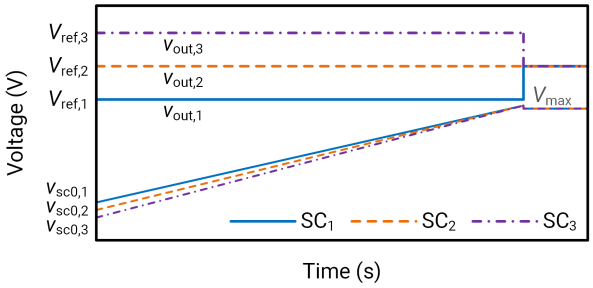

Fig. 6. The converter output voltage $v_{\text{out},j}$ must correspond to the initial supercapacitor voltage $v_{\text{sc},j}$ based on ΔE_j to provide balancing (to scale)

With (5), (9), and (12), we have the equations needed to control the modular power converters and balance supercapacitor voltages. This operation when control saturation is not a problem is referred to as the normal mode in the next sections. The steps in the flowchart in Fig. 5 are used in applying them.

To illustrate the strategy, we have in Fig. 6 an idealized example. Following the algorithm in Fig. 5, we obtain values of converter output voltages that total $V_{\text{ref,total}}$. Because SC_1 has the highest initial voltage, its converter should receive the lowest power share through the lowest converter output voltage based on the strategy. On the other hand, the converse is true for SC_3, which has the lowest initial voltage and thus the highest power share.

D. Control Saturation

The control of a modular power converter in Fig. 2 is said to be saturated when the duty ratio limits are already reached, but the voltage-balancing strategy still demands a value even beyond them. Fig. 6 illustrates an idealized application of the strategy. As the voltages for converter 1 show, the modular converter system is especially vulnerable to control saturation during balancing. Say that $v_{\text{sc0},1}$ is higher than in the figure. Because $-v_{\text{sc},j}^2$ is proportional to ΔE_j based on (5), while $v_{\text{out},j}$ is proportional to ΔE_j based on (8), $v_{\text{out},1}$ would have to be even lower than in the figure, increasing the chances of the case $v_{\text{out},1} = v_{\text{sc},1}$ happening before $v_{\text{sc},1}$ reaches V_{max} much more likely. In general, this means that the worse the supercapacitor voltage imbalance is, the greater the probability of control saturation.

As previously mentioned, control saturation would not be a problem if there is enough voltage margin in the system, i.e., the voltage ranges of the input and output sides do not coincide. However, the architecture constrains the system because (i) the converter structure discounts a high conversion ratio $M_j\,(D_j)$ because efficiency suffers with high $M_j\,(D_j)$, as will be shown in subsection A in section IV; (ii) using the full SoE range means an almost full use of the D_j range, again underscoring the need for a low $M_j\,(D_j)$; and (iii) worse imbalance entails further deviation from the nominal power share $V_{\text{ref,total}}/n$. Control saturation should thus happen quite frequently when trying to achieve the twin goals of charging and balancing supercapacitors.

So what happens when the control of a converter is saturated? Fig. 7 illustrates the same case as in Fig. 6, but

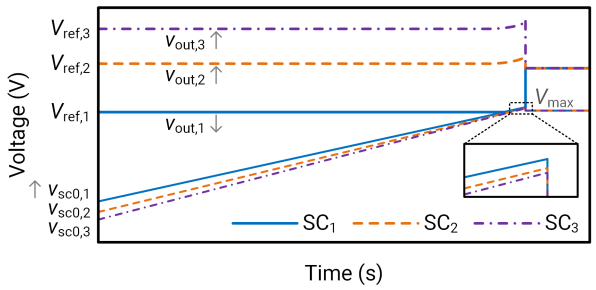

Fig. 7. A small increase in $v_{\mathrm{sc0,1}}$ results in saturation in the control of converter 1 before reaching $V_{\max}$ (to scale)

with a slightly higher value of $v_{\mathrm{sc0,1}}$. We can observe that due to this, the reference voltage for converter 1 is lower resulting in control saturation for converter 1 and in higher reference voltages for the remaining two converters. In the zoomed inset, we can also see that by the time they reach $V_{\max}$, the supercapacitor voltages are not yet balanced. This second case demonstrates that the current strategy is prone to control saturation. Once saturated, it can no longer achieve the stated twin goals of charging and balancing.

III. Strategy Adaptation to Control Saturation

In this section, we will first develop the general idea of adapting the voltage-balancing strategy to the problem of saturation and then advance modifications in the algorithm of the strategy.

A. Adapting the Strategy

We saw in the previous section that the problem of control saturation in modular converter circuits is basically due to the overlap between the ranges of the low-side and high-side voltages when charging while at the same time balancing. In such a scenario, the converters are in buck mode and control saturation is approached as $D_j \to 1^-$ and occurs when $v_{\mathrm{out},j} = v_{\mathrm{sc},j}$.

It is possible to modify the normal mode of the voltage-balancing strategy to consider control saturation. If we know that a converter will saturate at any point within the charging period, then we can saturate it on purpose from the start. We do this to correct and increase the amount of energy the supercapacitors connected to the converters that we know will never saturate get. Seen from this angle, the supercapacitor connected to a converter that eventually saturates gets more than its fair share of energy, as is the case in Fig. 7. The modified strategy will deduct the energy at the beginning. The challenge in implementing this method is that we must know which converters will eventually saturate.

If supercapacitor state of charge (SoC) were instead used in the strategy, control saturation cannot be accounted for in balancing supercapacitor voltages. The reason for this is that in considering the SoE in (4), the total energy needed to arrive at the rated voltage (when charging) is known and prediction of control saturation is possible. It thus becomes possible to adjust the power share of the converters that will saturate to achieve voltage equalization goals. In supercapacitors, the SoE is also a more useful metric because measuring the voltage allows one to readily calculate the SoE. On the other hand, current is the important parameter for batteries that allows calculation of the SoC [37].

B. Proposed Scheme

The weighting factor in (9) was specially defined to be constant throughout the charging period by considering the individual and total energies needed to charge the supercapacitors. The converters should thus have constant output voltages. We can then use the weighting factor to know which converters will eventually saturate.

Let us again consider the system in Fig. 2. How do we predict which converters will saturate? Remember that control saturation occurs when $v_{\mathrm{out},j} = v_{\mathrm{sc},j}$. Therefore, if supercapacitor j charges fully to $V_{\max}$ at the end of the charging period and control saturation is reached, $v_{\mathrm{out},j} = V_{\max}$ at that point. In fact, $V_{\max}$ serves as a boundary separating saturated converters $(v_{\mathrm{out},j} \leq V_{\max})$ from those that are not $(v_{\mathrm{out},j} > V_{\max})$. Since the reference converter output voltages and the weighting factors of the strategy are constant, they must have the same value even at the beginning of the charging period. First, we define a base weighting factor $w_{1(\mathrm{base}),j}$ computed from (9) considering all converters in the summation in the denominator (without regard for control saturation). The "1(base)" in $w_{1(\mathrm{base}),j}$ was added in the suffix as an additional qualifier to denote that we are currently in the first check and that it is the base weighting factor, i.e., the value of the weighting factor before the first check. The concept of checks will be developed in the next paragraphs. Based on (12), where $w_j = V_{\mathrm{ref},j}/V_{\mathrm{ref,total}}$, and on $V_{\max}$ serving as the boundary, we can also define a base threshold weight $w_{1(\mathrm{th})}$, where "th" in the suffix is for threshold, that we can use to predict whether a converter will eventually saturate or not:

$$w_{1(\mathrm{th})} = \frac{V_{\max}}{V_{\mathrm{ref,total}}} \tag{13}$$

As just discussed, if the inequality $v_{\mathrm{out},j} \leq V_{\max}$ is true for converter j, we know that this converter will eventually saturate. We can express this inequality in terms of weighting factors using (12) again: as a first check, if $w_{1(\mathrm{base}),j} \leq w_{1(\mathrm{th})}$, then converter j will saturate; otherwise, it will not. We could then deliberately saturate the converters that satisfied the condition. For these converters, the reference voltage becomes: $V_{\mathrm{ref},j} = r_{\mathrm{sat}} v_{\mathrm{sc},j}$, where r_{sat} is a factor slightly greater than unity. They are also removed from the application of the strategy to the remaining converters that will not saturate. They are also included in the set S, which is the set of all converters that we just predicted will saturate and whose size is $n_{S,1}$. If converter j will saturate, then $j \in S$. The converters contained in S are also removed from the application of the strategy to the remaining converters that will not saturate. For the latter, the reference voltage becomes:

$$V_{\mathrm{ref},j} = \left(V_{\mathrm{ref,total}} - \sum_{m \in S} V_{\mathrm{ref},m} \right) w_{1,j} \tag{14}$$

where $j \notin S$ and $w_{1,j}$ is the weighting factor computed by not including the $n_{S,1}$ converters in S from the summation in the denominator of (9).

Consider how the energy needed to charge a supercapacitor is calculated in (5). ΔE_j tends to decrease as $v_{\mathrm{sc},j} \to V_{\max}$ during a charge. For deliberately saturated converters contained in set S, the rate of decrease of ΔE_j is less than the rate of decrease of the remaining converters that are not saturated. This has an effect on how the weighting factors behave as defined in (9). Remember that when we add all of them, the sum must always be 100%. If that is the case, then the weighting factor $w_{1(\mathrm{base}),j}$ of deliberately saturated converters would just increase because of the smaller rate of decrease of ΔE_j during the charge. On the other hand, the $w_{1(\mathrm{base}),j}$ of the remaining converters would decrease. We can then stop deliberately saturating converters when all have $w_{1(\mathrm{base}),j} > w_{1(\mathrm{th})}$.

In other words, deliberately saturated converters increase their power share (expressed as $w_{1(\mathrm{base}),j}$ during the charge). On the other hand, the remaining converters that are not saturated decrease theirs. This attribute of the strategy opens to a possible problem. What if the converters that in the beginning will not saturate suddenly have $w_{1(\mathrm{base}),j} \leq w_{1(\mathrm{th})}$ because of their decreasing power share? How do we predict from the start that they will also undergo control saturation even though $w_{1(\mathrm{base}),j} > w_{1(\mathrm{th})}$ originally? Here, we define the next threshold weight $w_{2(\mathrm{th})}$ to do it:

$$w_{2(\mathrm{th})} = \frac{V_{\max}}{V_{\mathrm{ref,total}} - n_{S,1} V_{\max}} \tag{15}$$

where $n_{S,1}$ is the number of converters that will saturate based on the first check and the "2" in the suffix denotes second check. For this check, we verify if the condition $w_{2(\mathrm{base}),j} \leq w_{2(\mathrm{th})}$, where $j \notin S$, is true. The base weighting factor for the second check $w_{2(\mathrm{base}),j}$ considers only those converters that will not saturate based on the first check. The $n_{S,1}$ converters are thus excluded from the new computation of (9). Like in the previous step, we also deliberately saturate converters based on the condition through the reference voltage: $V_{\mathrm{ref},j} = r_{\mathrm{sat}} v_{\mathrm{sc},j}$. For the remaining converters that will not saturate, the reference voltage is:

$$V_{\mathrm{ref},j} = \left(V_{\mathrm{ref,total}} - \sum_{m \in S} V_{\mathrm{ref},m} \right) w_{2,j} \tag{16}$$

where S now includes converters from the second check and $w_{2,j}$ is the weighting factor computed by removing all converters in S from the summation in the denominator of (9).

In general, we can continue the process for the third check, fourth check, and so on until the last possible $(n-1)$th check. To summarize, the steps of the control saturation-adapted voltage-balancing strategy are:

1) For the time step Δt, perform $(n-1)$ checks. At each kth check, where $k \in \{1, 2, \ldots, n-1\}$, compute $w_{k(\mathrm{base}),j}(t)$ first:

$$w_{k(\mathrm{base}),j}(t) = \frac{\Delta E_j(t)}{\sum_{m \in U-S} \Delta E_m(t)} \tag{17}$$

where U is the set of all converters and S is the set of all converters within U that will surely saturate $(S \subseteq U)$. Note that $S = \emptyset$ when $k = 1$.

2) Within the same kth check, compute $w_{k(\mathrm{th})}(t)$ as well:

$$w_{k(\mathrm{th}),j}(t) = \frac{V_{\max}}{V_{\mathrm{ref,total}} - n_{S,k-1} V_{\max}} \tag{18}$$

3) Verify that $w_{k(\mathrm{base}),j}(t) \leq w_{k(\mathrm{th})}(t)$ for $j \notin S$ for the kth check. If true, update set S to include converter j. Then, proceed to the next check.

4) After the $(n-1)$ checks, deliberately saturate the converters in S according to $V_{\mathrm{ref},j}(t) = r_{\mathrm{sat}} v_{\mathrm{sc},j}(t)$, where r_{sat} is slightly greater than unity. The remaining converters in the set $U - S$ are then controlled according to:

$$V_{\mathrm{ref},j}(t) = \left[V_{\mathrm{ref,total}} - \sum_{m \in S} V_{\mathrm{ref},m}(t) \right] w_{n-1,j}(t) \tag{19}$$

5) Repeat steps 1–4 for the next time steps until the supercapacitors reach $V_{\max}$.

Fig. 8 represents the steps above for the control saturation-adapted energy-based strategy as a flowchart. Fig. 9 shows that

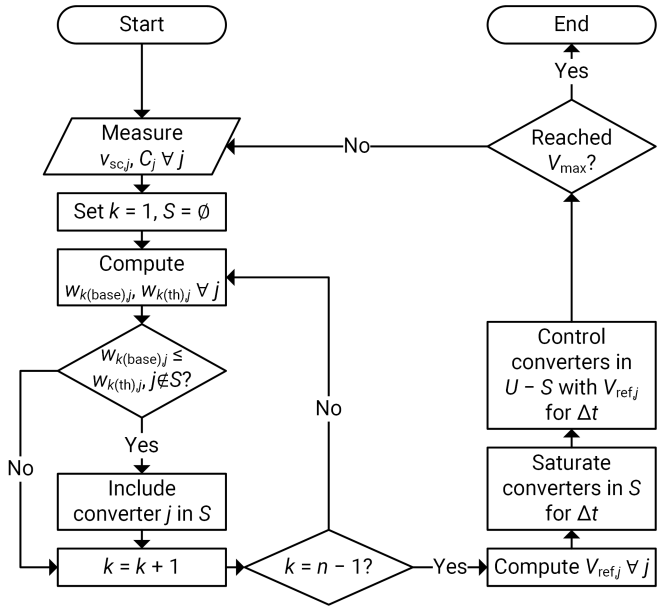

Fig. 8. Flowchart of the control saturation-adapted voltage-balancing strategy algorithm

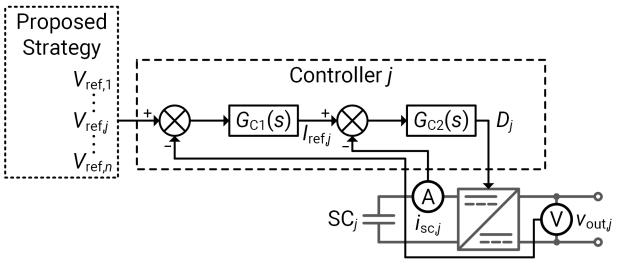

Fig. 9. Block diagram of the module-level control system and the proposed strategy

TABLE I
SUPERCAPACITOR (SC) GROUP PARAMETERS

Parameter	Variable	Simulation Value	Experiment Value
Group max. voltage (V)	$V_{\max}$	32.4	10
Group min. voltage (V)	$V_{\min}$	16.2	6.2
No. of cells in string	–	12	4

TABLE II
SUPERCAPACITOR (SC) CELL PARAMETERS

SC group	Simulation C (F)	Simulation ESR (mΩ)	Experiment C (F)	Experiment ESR (mΩ)
Variable	$C_{\rm sc}$	$R_{\rm sc}$	$C_{\rm sc}$	$R_{\rm sc}$
	Case study 1			
SC_1	262.5	3.31	6.25	64
SC_2	250	3.48	6.25	64
SC_3	237.5	3.65	6.25	64
	Case study 2			
SC_1	258.67	3.39	–	–
SC_2	249.67	3.23	–	–
SC_3	249.42	3.15	–	–
SC_4	236.7	4.21	–	–
SC_5	266.98	3.96	–	–
SC_6	247.78	3.57	–	–
SC_7	238.09	3.11	–	–
SC_8	272.53	3.23	–	–
SC_9	246.25	3.43	–	–
SC_{10}	240.18	3.71	–	–

the resulting $V_{{\rm ref},j}$ from the strategy serves as reference to the module-level control in Fig. 2(b). Adapting the basic strategy in subsection C in section II basically entailed predicting which converters will saturate. These converters are then deliberately saturated at the beginning to decrease their overall energy share and achieve voltage equalization at the end. The proposed strategy with its prediction of all converters that will eventually saturate by exhausting through threshold checks is a unique take on this unique problem. It is a novel contribution to the literature on voltage-balancing strategies. To strenghten this contribution, the proposed strategy will be compared with a conventional one in subsection B in section IV.

If the proposed strategy were applied to batteries, the control demonstrated as the converter output voltages would not be different. However, because battery voltage relative to its SoC is comparatively flat (unlike in supercapacitors), the case of control saturation in batteries is less common. However, if second-life batteries with different states of health were instead used in the same architecture, the proposed strategy would be advantageous to use.

IV. SIMULATION

We simulated the system and the strategy as described in the previous two sections. To demonstrate the operation of the strategy, we modelled a 50-kW system and tested it and compared it with a conventional strategy in simulation.

A. Simulation Setup

1) System Sizing: We modelled and simulated the modular power converter system as represented in Fig. 2(a). The sizing of the modular converters follows from the previous study that used a single 50-kW converter to interface 120 3,000-F supercapacitor cells in recovering the breaking energy and in supplementing power during electrical microcuts in a trolleybus [26]. Temperature is important in the evolution of cell capacitance and ESR, but it is difficult to ensure thermal homogeneity in a supercapacitor stack [38]. Cells were thus grouped according to their thermal behavior to ensure that voltage imbalance within a group is kept minimal. Following this, we decided to group the supercapacitors by 12. SC_j in Fig. 2(a) can thus be treated as the equivalent supercapacitor of 12 cells connected in series. For simplicity, only three converters $(n = 3)$ were considered for case study 1, while case study 2 has the full sizing $(n = 10)$ considered. The characteristics of the supercapacitors within a group were considered uniform. Table I gives the group operating voltage range of the 3,000-F supercapacitors used in the simulation of the test cases. Each supercapacitor cell is limited in use within the usual 1.35–2.7 V range. On the other hand, Table II provides the different values of group *RC* model parameters to replicate the tolerance in nominal values of real supercapacitors. For case study 1, values for SC_1 and SC_3 were set to be ±5% of the values for SC_2. For case study 2, normally distributed random values were generated based on a tolerance of ±20% for the cell capacitance (mean $\mu = 3,000$ F; standard deviation $\sigma = 0.2\mu/3$ F) and ±25% for the cell ESR ($\mu = 0.29$ mΩ; $\sigma = 0.25\mu/3$ mΩ).

TABLE III
MODULAR POWER CONVERTER AND SYSTEM SPECIFICATIONS

Parameter	Variable	Simulation Value	Experiment Value
Switching f (kHz)	f_s	10	50
System output i (A)	$i_{\rm out,max}$	±143	±0.857
Test system output i (A)	$i_{\rm out}$	±50	±0.4
Conv. nominal output v (V)	$v_{\rm out}$	35	11.67
Conv. input v range (V)	$v_{\rm in}$	16.2–32.4	5.4–10.8
Conv. inductor (μH)	L	16	1,300
Conv. inductor ESR (mΩ)	R_L	0.65	–
Conv. capacitor (μF)	C_C	16,000	30
Conv. capacitor ESR (mΩ)	R_C	10	–
MOSFET on R (mΩ)	$R_{\rm DS(on)}$	3.9	–
Bal. strategy time step (s)	Δt	0.2	0.2
System power rating (W)	$P_{\max}$	50,000	30
Test system power (W)	P	17,500	14
System bus voltage $V_{\rm bus}$ (V)	$V_{\rm ref,total}$	105 or 350	35
No. of cascaded converters	n	3 or 10	3

Following still the partitioning of the original 50-kW system, the specifications of the modular converters are detailed in Table III. Each converter nominally has 35 V at the output, so the regulation of the bus voltage $V_{\rm ref,total}$ was set at 105 V for case study 1 and 350 V for case study 2, while the charging current was set at $i_{\rm out} = 50$ A. The three converters in case study 1 processed 5.25 kW of power in total, while the ten converters in case study 2 processed 17.5 kW in total. The voltage-balancing strategy was applied to the system with a time step of $\Delta t = 0.2$ s.

2) Use of the Strategy and Efficiency: Simulation of the system was done in Simscape, an environment within MATLAB and Simulink for multidomain physical modelling and simulation. At the modular converter level in Fig. 1(a), control

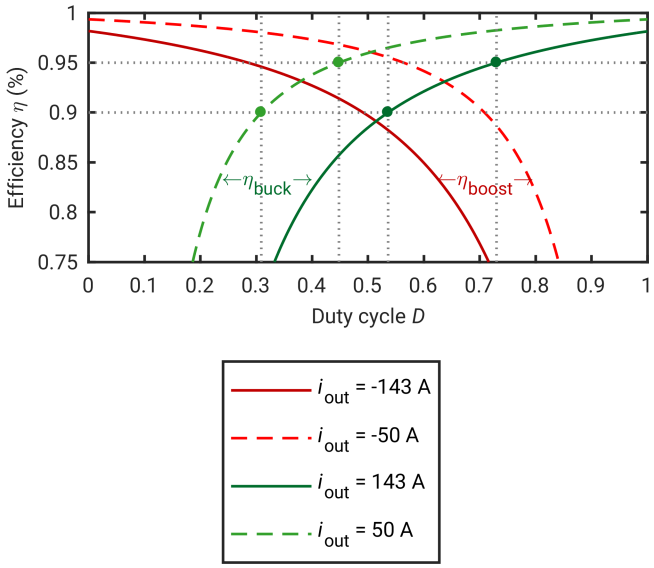

Fig. 10. Bidirectional converter efficiency as a function of duty ratio and load: green represents charging supercapacitors (buck mode) and red represents discharging (boost mode)

of switches Q_1 and Q_2 are synchronous or complementary, i.e. Q_1 is on when Q_2 is off and vice versa. Based on this, a unified state space average model was derived for both the boost and buck modes [32]. It gave us the transfer functions in (1) and (2), which, in turn, were used to design controllers $G_{C1}(s)$ and $G_{C2}(s)$ respecting the set loop response times mentioned in subsection A in section II through the Control System Designer in MATLAB. Table III shows the dc values in (1) and (2), with D set at 0.35 to get a V_{in} in the middle of the range. Also based on the same model, the supercapacitor current at steady state can be represented as:

$$i_{\text{in}} = \frac{i_{\text{out}}}{D} \tag{20}$$

On the other hand, the steady-state converter output voltage can be formulated as:

$$v_{\text{out}} = \frac{v_{\text{in}}}{D} + i_{\text{out}} \left[\frac{R_L + R_{\text{DS(on)}} + R_C D\,(1-D)}{D^2} \right] \tag{21}$$

This last expression shows the effects of the parasitic resistances. In the ideal scenario without them, v_{out} can be reduced into just the first term of (21). Thus, given values for v_{in} and v_{out}, the duty ratio can be approximated as:

$$D \approx \frac{v_{\text{in}}}{v_{\text{out}}} \tag{22}$$

Still based on the steady-state behavior of the converter in (20) and (21), the expression for the buck mode efficiency η_{buck} considering only conduction losses can also be obtained:

$$\eta_{\text{buck}} = \frac{P_{\text{in}}}{P_{\text{out}}} = 1 - \frac{i_{\text{out}}}{v_{\text{out}}} \left[\frac{R_L + R_{\text{DS(on)}} + R_C D\,(1-D)}{D^2} \right] \tag{23}$$

To see the effects of loading and the duty ratio on the efficiency, the plot of (23) in different conditions is shown in Fig. 10. Curves for the boost mode efficiency η_{boost} are also shown.

Considering first the full-rated load in buck mode where $i_{\text{out}} = 143$ A, the duty ratio should be $D_{\text{buck}} \geq 0.54$ to achieve at least 90% efficiency. The range of duty ratio values that is at least 90% efficient increases as i_{out} decreases because of the inverse relationship between the current and the load. This means that a lower i_{out} is preferred when using the voltage-balancing strategy to charge supercapacitors. In applications however, charging time should be balanced against the choice of a lower charging current and a higher efficiency.

For the case study-rated load of $i_{\text{out}} = 50$ A in Fig. 10, $D_{\text{buck}} \geq 0.31$ for at least 90% efficiency and $D_{\text{buck}} \geq 0.45$ for at least 95%. Assuming a nominal output voltage $v_{\text{out}} = 35$ V, these correspond to an $SoE \approx 11.2\%$ ($v_{\text{sc}} = 0.9$ V per cell) and an $SoE \approx 23.6\%$ ($v_{\text{sc}} = 1.3$ V per cell), respectively. This means that the SoE could be as low as 11% at the beginning of the charging period and the efficiency would still be at least 90%. As the supercapacitors charge, v_{in} will only increase and further improve the efficiency according to (22) and (23). Note however that the preceding analysis has underestimated values because other sources of losses were not considered.

TABLE IV
SUPERCAPACITOR (SC) INITIAL CONDITIONS

Supercapacitor group	Simulation initial voltage (V)	Experiment initial voltage (V)
	Case study 1	
SC_1	26.4	7.47
SC_2	25.8	7.24
SC_3	23.4	6.01
	Case study 2	
SC_1	24.46	–
SC_2	23.36	–
SC_3	26.13	–
SC_4	23.14	–
SC_5	23.7	–
SC_6	27.96	–
SC_7	24.81	–
SC_8	25.31	–
SC_9	27.18	–
SC_{10}	25.02	–

B. Simulation Results and Discussion

The two case studies have different initial voltages given in Table IV. Values for case study 1 were chosen to demonstrate the operation of the control saturation-adapted strategy in comparison to a conventional one, while cell values for case study 2 were normally distributed random numbers ($\mu = 2.13$ V; $\sigma = 0.1$ V).

1) Simulation Case Study 1—Comparison with a Conventional Voltage-Balancing Strategy on a Three-Converter System: In this first case study (cf. Tables I–IV), a converter is expected to enter control saturation during charging. The results are shown in Fig. 11. We can see in Fig. 11(a) that the control saturation-adapted strategy was effective in balancing the voltages at 29 s. Doing the two checks with an added hysteresis band about the threshold to prevent chattering, the strategy decided that two converters had to be deliberately

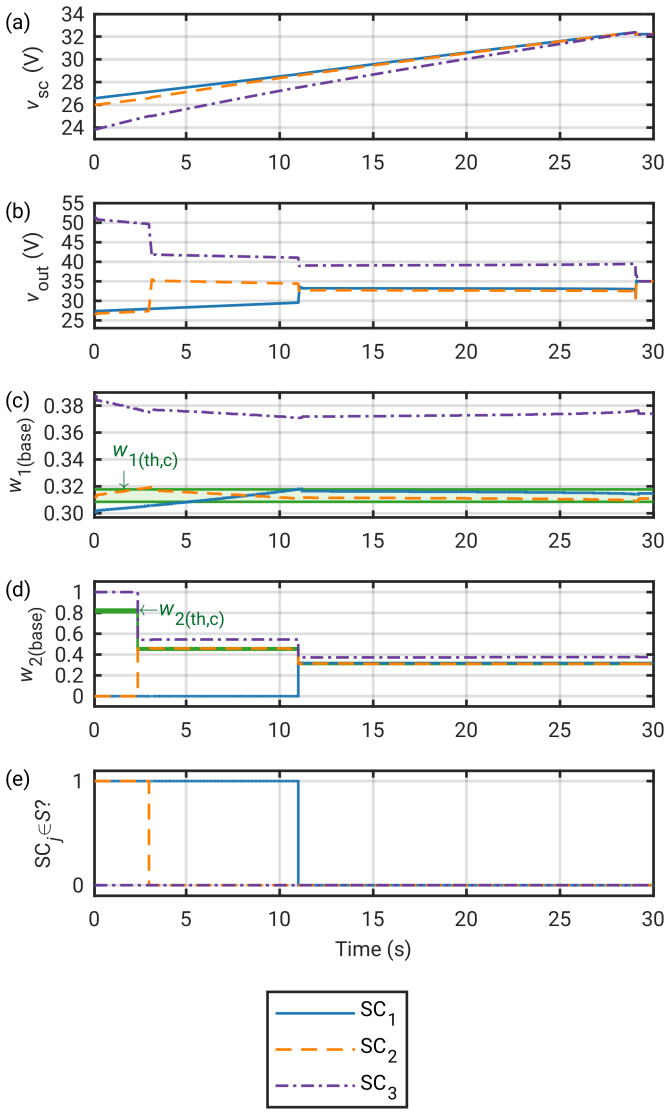

Fig. 11. Simulation case study 1: (a) Supercapacitor voltages $(v_{\mathrm{sc},j})$; (b) Output voltages of the converters $(v_{\mathrm{out},j})$; (c) Weighting factors $(w_{1(\mathrm{base}),j})$ for the first check $(k = 1)$; (d) Weighting factors $(w_{2(\mathrm{base}),j})$ for the second check $(k = 2)$; and (e) Result of the two checks on whether to saturate converter j.

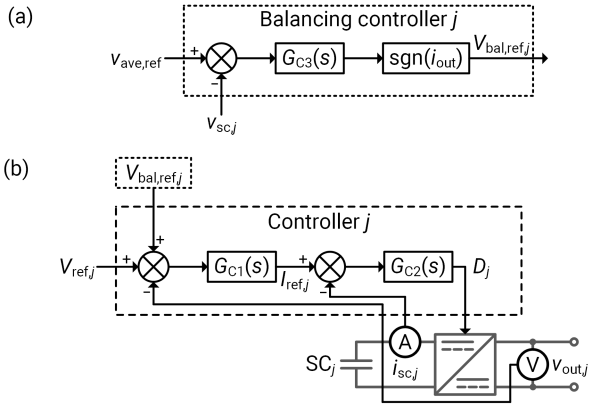

Fig. 12. Block diagram of a conventional voltage-balancing strategy: (a) Control system and (b) Connection to module-level control

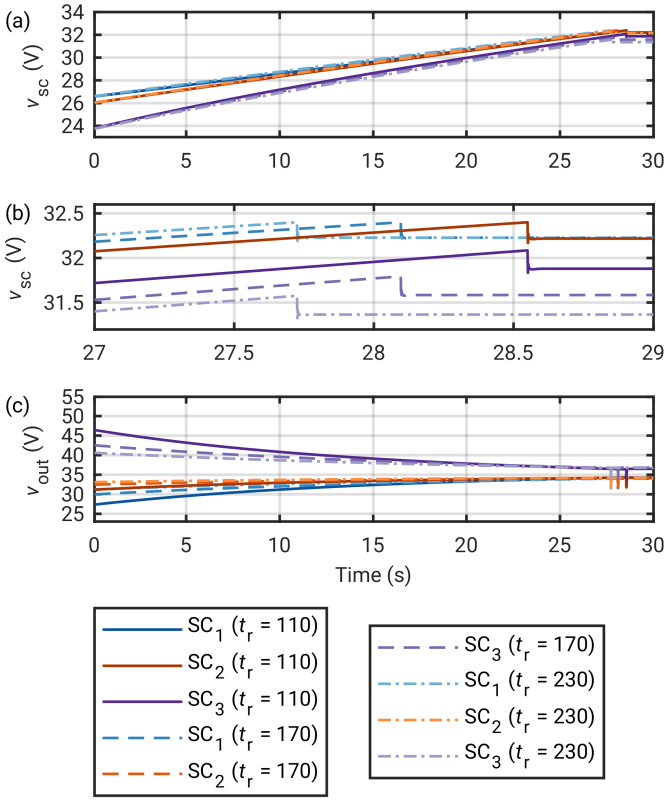

Fig. 13. Conventional voltage-balancing strategy with different response times (t_r): (a) Supercapacitor voltages $(v_{\mathrm{sc},j})$; (b) Zoomed maximum and minimum supercapacitor voltages $(v_{\mathrm{sc},j})$; and (c) Output voltages of the converters $(v_{\mathrm{out},j})$.

saturated: 1 and 2. Beyond 3 s, only converter 1 needed to be deliberately saturated. At 11 s, all three weighting factors $(w_{1(\mathrm{base}),j})$ clear the two checks. Thereafter, the normal mode of the energy-based strategy operated to charge the supercapacitors until $V_{\max}$.

Converter 2 will not be released from saturation until after 3 s because the second check still showed in Figs. 11(d)–(e) that $w_{2(\mathrm{base}),2} \leq w_{2(\mathrm{th})}$ with hysteresis control. There was still a need to deliberately saturate it. The upper and lower threshold limits for the hysteresis control are not obvious because of the increased scale of the vertical axis, but $w_{2(\mathrm{base}),2}$ touches the upper threshold limit at 3 s. Another thing to observe in the second check in Fig. 11(d) is the dependence on the first check. For example, $w_{2(\mathrm{base}),j} = 0$ for converters to be deliberately saturated based on the previous check and $w_{2(\mathrm{th})}$ changes value depending on their number.

The proposed strategy was also compared to another voltage-balancing strategy developed and experimentally validated for supercapacitors [39]. The latter was inspired by another voltage-balancing strategy first proposed for batteries in a distributed battery energy storage system [14]. For purposes of comparison, we will treat the strategy of [39] as conventional because it did not consider control saturation. The related control system block diagrams are shown in Fig. 12.

As can be seen Fig. 12(a), the balancing controller aims to minimize the error between $v_{\mathrm{sc},j}$ and the average of all supercapacitor voltages $v_{\mathrm{ave,ref}}$. The speed of balancing can be controlled by adjusting the response time t_{r}, which is a parameter that controls the term of the proportional controller G_{C3} in Fig. 12(a) for the response to reach 95% of the final value. The conventional strategy was not originally designed for fast balancing [39], but as will be shown next, when similar strategies that do not consider control saturation are used for such purposes, the goals of (i) charging supercapacitors until $V_{\max}$, and (ii) reaching $V_{\max}$ at the same time cannot be achieved.

Results for different response times are shown in Fig. 13. Fig. 13(a) shows how the supercapacitor voltages are balanced as the conventional method is applied. The differences are not noticeable because of the scale, so the figure was zoomed in Fig. 13(b) as one of the supercapacitors reach $V_{\max}$. However, to decrease clutter, only the maximum and minimum supercapacitor voltages are shown. It can be observed that balancing is faster (i.e., the difference between the maximum and minimum values decrease) with smaller response times, which is as designed. Fig. 13(c) shows the converter output voltages. It can be seen that with faster balancing, $v_{\mathrm{out},1}$ becomes lower. However, we know from the previous sections that $v_{\mathrm{out},1}$ cannot go lower than $v_{\mathrm{sc},1}$. Otherwise, converter 1 will enter control saturation. In this case, $t_{\mathrm{r}} = 110$ s is already the lowest possible given the initial value of $v_{\mathrm{sc},1}$ without letting converter 1 enter control saturation. Still, the supercapacitor voltages are not balanced by the time $v_{\mathrm{sc},1}$ reached $V_{\max}$. The preceding discussion shows the limitations of conventional balancing strategies in dealing with control saturation. The proposed control saturation-adapted strategy provides a solution to these limitations.

2) Simulation Case Study 2—Ten-Converter System: The supercapacitors have different initial voltages. The case study (cf. Tables I–IV) demonstrates a limitation of the control saturation-adapted strategy. The results are shown in Fig. 14. It is obvious from Fig. 14(a) that while SC_6 already reached $V_{\max}$, the others have not. The strategy could not work with the combination of initial voltages. In such a case, it is still possible to balance the voltages. However, it will have to take more time. The plan is to apply the strategy even during discharge. To do this, ΔE_j in (5) must be modified to:

$$\Delta E_j\left(t\right) = \frac{1}{2} C_{\mathrm{sc},j}\left[v_{\mathrm{sc},j}^2\left(t\right) - V_{\min}^2\right] \tag{24}$$

for the discharge period. $V_{\min} = V_{\max}/2$ refers to the rated minimum operating voltage of the supercapacitor. Accordingly, the threshold in (18) must be modified to reflect discharging during this period:

$$w_{k(\mathrm{th}),j}\left(t\right) = \frac{V_{\min}}{V_{\mathrm{ref,total}} - n_{S,k-1} V_{\min}} \tag{25}$$

We can see in Figs. 14(b)–(c) that five converters (3, 6, 7, 9, and 10) were deliberately saturated at the very start. The supercapacitors connected to them required lower energy shares in order for the strategy to balance the system. One by one, the deliberately saturated converters are released from saturation based on the nine checks: converter 7 at 3.2 s; converter 10 at 6.2 s; and the other three (converters 3, 6, and 9) at the point where SC_6 reached $V_{\max}$ at 20.7 s. This case study shows that the proposed control saturation-adapted strategy can be used as a general fast voltage-balancing strategy for both charging and discharging periods and that the strategy works for larger systems.

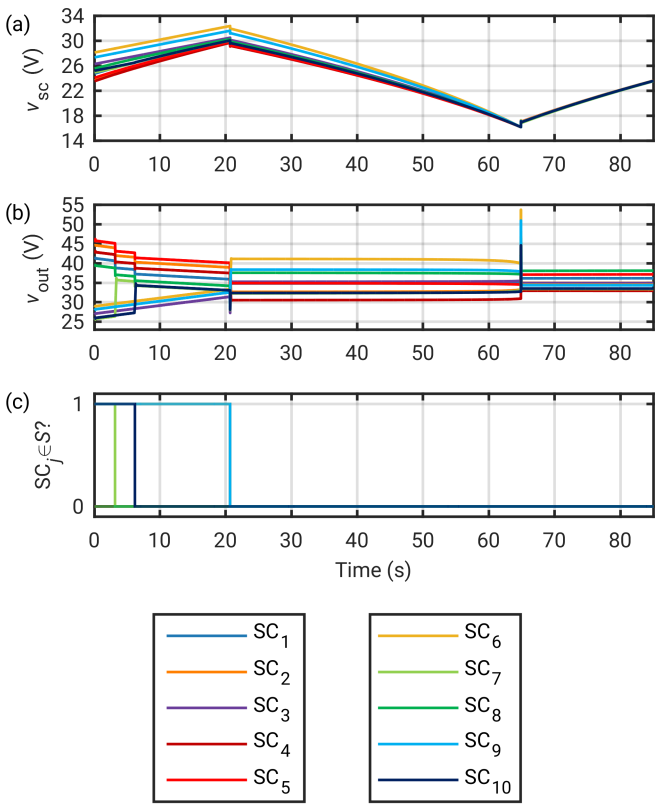

Fig. 14. Simulation case study: (a) Supercapacitor voltages $(v_{\mathrm{sc},j})$; (b) Output voltages of the converters $(v_{\mathrm{out},j})$; and (c) Result of the nine checks on whether to saturate converter j.

V. Experimental Results

The strategy was also experimentally implemented on a small-scale 30-W system with three modular converters. We look at the experimental case study in detail in this section.

A. Experimental Setup

A small-scale 30-W prototype of a bidirectional modular converter system with supercapacitor energy storage represents the system in Fig. 2(a) and serves as a test bench for the experimental implementation of the voltage-balancing strategy [39]. The modular converters were controlled by a Speedgoat real-time target machine that interacted with its workstation user interface through Simulink Real-Time Explorer. The control system in Fig. 2(b) was programmed into the target machine using MATLAB and Simulink. All the control and data acquisition functions are taken care of by the target machine. Fig. 15 shows an image of the experimental setup. It is the prototype of the system in Fig. 2.

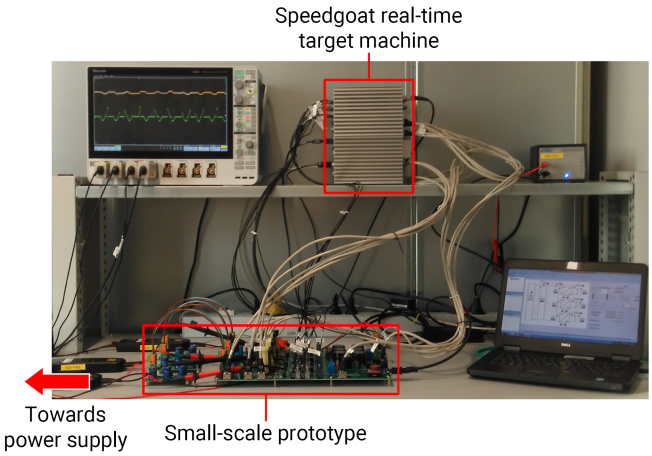

Fig. 15. The experimental setup of a small-scale prototype of modular converters with connected supercapacitors

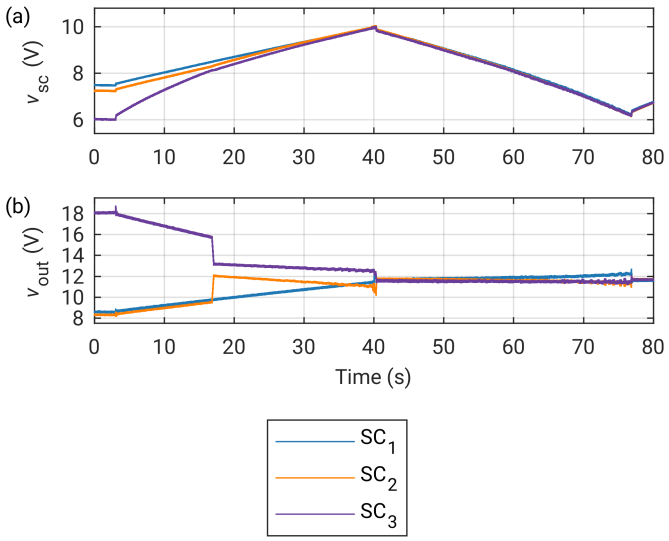

Fig. 16. Experimental case study: (a) Supercapacitor voltages and (b) Output voltages of the converters

Connected to each modular converter in the prototype is a supercapacitor group composed of a string of four 25-F cells. Table I shows the group operating voltage range while Table II provides the *RC* model parameters of the superpacitors. Three modular converters comprise the prototype and each converter has a nominal output voltage of 11.67 V. Bus regulation $V_{\mathrm{ref,total}}$ was set at 35 V, while charging current was set at $i_{\mathrm{out}} = 400$ mA. Specifications of the modular power converters and of the experimental setup are detailed in Table III.

B. Experimental Results and Discussion

Like in the simulation case study, the initial voltages of the supercapacitors were set at different values to demonstrate the operation of the proposed strategy. These values can be in Table IV. This experimental test case (cf. Tables I–IV) demonstrates the operation of the control saturation-adapted voltage-balancing strategy. Fig. 16 shows the experimental results. Unlike the ideal case and the simulation case studies, the output voltages in this experimental case are not constant. This is most obvious for $v_{\mathrm{out},1}$ in Fig. 16(b). In reality, the capacitance depends on supercapacitor voltage, but the *RC* model assumes that $C_{\mathrm{sc},j}$ in (5) is a constant [40]. A higher r_{sat} serves not only to secure the prototype during transients, but also to account for the nonconstant output voltages during times of no saturation (normal mode). A higher r_{sat} means a larger difference between $V_{\max}$ and $v_{\mathrm{out},j}$. Even if $v_{\mathrm{out},1}$ were to go higher during the normal mode, there would still be enough voltage difference between it and $v_{\mathrm{sc},2}$ thus ensuring that the supercapacitor voltages were balanced. Despite the nonconstant converter output voltages, the strategy still works.

The supercapacitor voltages are completely balanced by the time they reach 6.2 V at the 77-s mark, as shown in Fig. 16(a). Like in the corresponding simulation case studies, this experimental case study shows that the control saturation-adapted strategy can be used as a general fast voltage-balancing strategy that works in both charging and discharging periods.

VI. Conclusion

The case studies show the principles of operation and limitations of the proposed strategy for modular power converter balancing. Its use was initially limited by the difficulty of adapting it to control saturation. On the other hand, its features of constant weighting factors and constant converter output voltages made it easier in rendering it adaptable to control saturation. The proposed way works by deliberately saturating converters. Doing such corrects the energy shares to make the normal mode of the energy-based strategy work. The results show that the proposed strategy can be used as a fast voltage-balancing strategy during the supercapacitor charging period or as a general fast method even during discharge when balancing during a single charging period is not possible, regardless of system size.

References

[1] A. Rufer, *Energy Storage: Systems and Components*. Boca Raton, FL, USA: CRC Press, Taylor & Francis Group, 2018.
[2] L. Zhang, X. Hu, Z. Wang, F. Sun, and D. G. Dorrell, "A review of supercapacitor modeling, estimation, and applications: A control/management perspective," *Renew. Sustain. Energy Rev.*, vol. 81, pp. 1868–1878, Jan. 2018.
[3] F. Béguin and E. Frackowiak, *Supercapacitors: Materials, Systems, and Applications*. Weinheim, Germany: Wiley-VCH Verlag GmbH & Co., 2013.
[4] S. Zhang and N. Pan, "Supercapacitors Performance Evaluation," *Adv. Energy Mater.*, vol. 5, no. 6, p. 1401401, Mar. 2015.
[5] "Product Guide: Maxwell Technologies BOOTSCAP Ultracapacitors," Maxwell Technologies, Inc., Product Guide, 2009.
[6] "Murata Supercapacitor Technical Note," Murata Manufacturing Co., Ltd., Technical Note.
[7] D. Linzen, S. Buller, E. Karden, and R. DeDoncker, "Analysis and Evaluation of Charge-Balancing Circuits on Performance, Reliability, and Lifetime of Supercapacitor Systems," *IEEE Trans. Ind. Appl.*, vol. 41, no. 5, pp. 1135–1141, Sep. 2005.
[8] P. Kreczanik, P. Venet, A. Hijazi, and G. Clerc, "Study of Supercapacitor Aging and Lifetime Estimation According to Voltage, Temperature, and RMS Current," *IEEE Trans. Ind. Electron.*, vol. 61, no. 9, pp. 4895–4902, Sep. 2014.

[9] F. M. Ibanez, "Analyzing the Need for a Balancing System in Supercapacitor Energy Storage Systems," *IEEE Trans. Power Electron.*, vol. 33, no. 3, pp. 2162–2171, Mar. 2018.

[10] Y. Diab, P. Venet, and G. Rojat, "Comparison of the Different Circuits Used for Balancing the Voltage of Supercapacitors: Studying Performance and Lifetime of Supercapacitors," in *Proc. 2nd Eur. Symp. Super Capacitors and Appl. (ESSCAP'06)*, Lausanne, Switzerland, Nov. 2006.

[11] J. Cao, N. Schofield, and A. Emadi, "Battery balancing methods: A comprehensive review," in *Proc. 2008 IEEE Vehicle Power and Propulsion Conf. (VPPC)*, Harbin, China, Sep. 2008.

[12] M. Hoque, M. Hannan, A. Mohamed, and A. Ayob, "Battery charge equalization controller in electric vehicle applications: A review," *Renew. Sustain. Energy Rev.*, vol. 75, pp. 1363–1385, Aug. 2017.

[13] F. Altaf, L. Johannesson, and B. Egardt, "On Thermal and State-of-Charge Balancing using Cascaded Multi-level Converters," *J. Power Electron.*, vol. 13, no. 4, pp. 569–583, Jul. 2013.

[14] W. Huang and J. A. Abu Qahouq, "Energy Sharing Control Scheme for State-of-Charge Balancing of Distributed Battery Energy Storage System," *IEEE Trans. Ind. Electron.*, vol. 62, no. 5, pp. 2764–2776, May 2015.

[15] N. Mukherjee, D. Strickland, and M. Abedi Varnosfaderani, "Adaptive Control of Hybrid Battery Energy Storage Systems under Capacity Fade," *EPE J.*, vol. 25, no. 4, pp. 25–33, Oct. 2015.

[16] N. Mukherjee and D. Strickland, "Control of Cascaded DC–DC Converter-Based Hybrid Battery Energy Storage Systems—Part I: Stability Issue," *IEEE Trans. Ind. Electron.*, vol. 63, no. 4, pp. 2340–2349, 2016.

[17] ——, "Control of Cascaded DC–DC Converter-Based Hybrid Battery Energy Storage Systems—Part II: Lyapunov Approach," *IEEE Trans. Ind. Electron.*, vol. 63, no. 5, pp. 3050–3059, 2016.

[18] M. Evzelman, M. M. U. Rehman, K. Hathaway, R. Zane, D. Costinett, and D. Maksimovic, "Active Balancing System for Electric Vehicles With Incorporated Low-Voltage Bus," *IEEE Trans. Power Electron.*, vol. 31, no. 11, pp. 7887–7895, Nov. 2016.

[19] F. Altaf, B. Egardt, and L. Johannesson Mardh, "Load Management of Modular Battery Using Model Predictive Control: Thermal and State-of-Charge Balancing," *IEEE Trans. Control Syst. Technol.*, vol. 25, no. 1, pp. 47–62, Jan. 2017.

[20] F. Altaf and B. Egardt, "Comparative Analysis of Unipolar and Bipolar Control of Modular Battery for Thermal and State-of-Charge Balancing," *IEEE Trans. Veh. Technol.*, vol. 66, no. 4, pp. 2927–2941, Apr. 2017.

[21] J. Leuchter, P. Bauer, P. Bojda, and V. Rerucha, "Bi-directional DC-DC converters for supercapacitor based energy buffer for electrical gen-sets," in *Proc. 2007 Eur. Conf. Power Electron. and Appl.*, Aalborg, Denmark, 2007.

[22] M. B. Camara, H. Gualous, F. Gustin, A. Berthon, and B. Dakyo, "DC/DC Converter Design for Supercapacitor and Battery Power Management in Hybrid Vehicle Applications—Polynomial Control Strategy," *IEEE Trans. Ind. Electron.*, vol. 57, no. 2, pp. 587–597, Feb. 2010.

[23] A. S. Samosir and A. H. M. Yatim, "Implementation of Dynamic Evolution Control of Bidirectional DC–DC Converter for Interfacing Ultracapacitor Energy Storage to Fuel-Cell System," *IEEE Trans. Ind. Electron.*, vol. 57, no. 10, pp. 3468–3473, Oct. 2010.

[24] D. Montesinos-Miracle, M. Massot-Campos, J. Bergas-Jane, S. Galceran-Arellano, and A. Rufer, "Design and Control of a

[29] N. Mukherjee and D. Strickland, "Analysis and Comparative Study of Different Converter Modes in Modular Second-Life Hybrid Battery Energy Storage Systems," *IEEE J. Emerg. Sel. Topics Power Electron.*, vol. 4, no. 2, pp. 547–563, Jun. 2016.

Modular Multilevel DC/DC Converter for Regenerative Applications," *IEEE Trans. Power Electron.*, vol. 28, no. 8, pp. 3970–3979, Aug. 2013.

[25] P. J. Grbović, *Ultra-capacitors in power conversion systems: applications, analysis and design from theory and practice*. Chichester, West Sussex, United Kingdom: IEEE Press/Wiley, 2014.

[26] A. Hijazi, E. Bideaux, P. Venet, and J.-P. Simon, "Sizing of supercapacitors stack: Application to the braking energy recovery of electrical bus," in *Proc. 4th Eur. Symp. Super Capacitors and Appl. (ESSCAP'10)*, Bordeaux, France, Oct. 2010.

[27] F. Errigo, L. Chédot, F. Morel, P. Venet, A. Sari, A. Hijazi, and R. A. Peña, "Assessment of Aging and Performance Degradation of Supercapacitors Integrated into a Modular Multilevel Converter," Lyon, France, Sep. 2020.

[28] F. Errigo, T. Lagier, L. Chédot, A. Sari, and P. Venet, "Multi-Level Voltage Converter with Optimised Additional Energy Storage," French Patent WO2 020 225 332A1, Nov., 2020.

[30] H. R. Karshenas, H. Daneshpajooh, A. Safaee, P. Jain, and A. Bakhshai, "Bidirectional DC-DC Converters for Energy Storage Systems," in *Energy Storage in the Emerging Era of Smart Grids*, R. Carbone, Ed. InTech, Sep. 2011.

[31] R. Kötz, J.-C. Sauter, P. Ruch, P. Dietrich, F. Büchi, P. Magne, and P. Varenne, "Voltage balancing: Long-term experience with the 250 V supercapacitor module of the hybrid fuel cell vehicle HY-LIGHT," *J. Power Sources*, vol. 174, no. 1, pp. 264–271, Nov. 2007.

[32] M. Bhardwaj, "Modeling Bi-Directional Buck/Boost Converter for Digital Control Using C2000 Microcontrollers," Texas Instruments Inc., Application Report, Jan. 2015.

[33] N. Devillers, S. Jemei, M.-C. Péra, D. Bienaimé, and F. Gustin, "Review of characterization methods for supercapacitor modelling," *J. Power Sources*, vol. 246, pp. 596–608, Jan. 2014.

[34] M. Mellincovsky, A. Kuperman, C. Lerman, I. Aharon, N. Reichbach, G. Geula, and R. Nakash, "Performance assessment of a power loaded supercapacitor based on manufacturer data," *Energy Convers. Manag.*, vol. 76, pp. 137–144, Dec. 2013.

[35] M. Mellincovsky, A. Kuperman, C. Lerman, S. Gadelovits, I. Aharon, N. Reichbach, G. Geula, and R. Nakash, "Performance and Limitations of a Constant Power-Fed Supercapacitor," *IEEE Trans. Energy Convers.*, vol. 29, no. 2, pp. 445–452, Jun. 2014.

[36] F. Odeim, J. Roes, and A. Heinzel, "Power Management Optimization of an Experimental Fuel Cell/Battery/Supercapacitor Hybrid System," *Energies*, vol. 8, no. 7, pp. 6302–6327, Jun. 2015.

[37] M. Ceraolo, G. Lutzemberger, and D. Poli, "State-Of-Charge Evaluation Of Supercapacitors," *Journal of Energy Storage*, vol. 11, pp. 211–218, Jun. 2017.

[38] A. Hijazi, E. Bideaux, P. Venet, and G. Clerc, "Electro-thermal sizing of supercapacitor stack for an electrical bus: Bond graph approach," in *Ecological Vehicles and Renewable Energies (EVER), 2015 Tenth International Conference on*. IEEE, 2015, pp. 1–8.

[39] F. Errigo, "Convertisseurs de puissance avec stockage d'énergie intégré pour réseaux haute tension à courant continu," PhD thesis, Université Claude Bernard Lyon 1, Université de Lyon, Villeurbanne, France, 2020.

[40] Y. Diab, P. Venet, H. Gualous, and G. Rojat, "Self-Discharge Characterization and Modeling of Electrochemical Capacitor Used for Power Electronics Applications," *IEEE Transactions on Power Electronics*, vol. 24, no. 2, pp. 510–517, Feb. 2009.